analytical chemistry

pubs.acs.org/ac Letter

A Novel Bifunctional Transparent Non-covalent Crosslinked Hydrogel for Wearable Sensors and Ion Detection

Jun Hu, Yuting Tian, Xiaoying Xin, Michael Daramola,* and Guodong Fu*

Cite This: *Anal. Chem.* 2025, 97, 25937−25945 Read Online

ACCESS | Metrics & More | Article Recommendations | Supporting Information

ABSTRACT: Currently, it is insufficient to solely detect physical signals for the flexible sensor as a wearable electronic. Conductive hydrogels can serve as the ideal candidate for designing a novel wearable sensor with multiple functionalities, which benefits from the nature of flexibility, biocompatibility, and modulated function. However, they are usually fabricated by the chemical crosslinking polymer network, leading to a low chain fluidity and brittleness resulting from the poor energy dissipation. Additionally, the time-consuming preparation process and use of toxic initiators also pose a significant challenge to them for practical application. Herein, we prepared a novel noncovalent crosslinked hydrogel-based sensor with the deep eutectic solvents (DES)-catalyzed initiator and crosslinker-free method triggered by sunlight, the resulting interpenetrating polymer network (IPN) hydrogel dopped with zinc oxide quantum dots (ZnO QDs) exhibited favorable transparency, mechanical performance, and reliable adhesion, which can be utilized to monitor daily physiological motion in real time and detect abnormal ions due to certain diseases, providing a new insight for the revolution of development principle versatile wearable electronic fields.

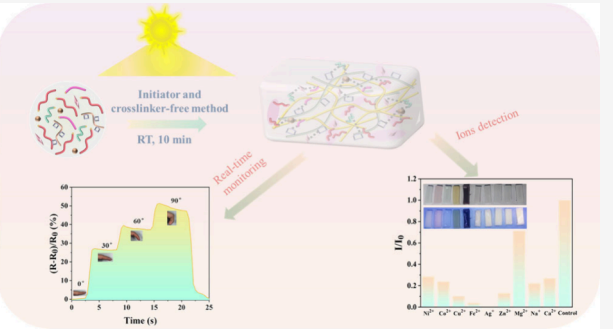

INTRODUCTION

With the rapid development of wearable electronics, flexible strain sensors have been extensively exploited in various fields, such as human−machine interfaces,[1] electronic skin,[2] and intelligent sports devices.[3,4] However, the existing sensors are usually constrained in detecting physical signals, including limb movement, heart rate, and blood pressure. The conception of the Internet of Everything (IoE) aroused an urgent requirement for flexible sensors with multifunctional applications, rendering conductive hydrogels the ideal candidate for wearable devices due to their flexibility, biocompatibility, designable structure, and function.[5,6]

The internal pathway for ionic transfer in a conductive hydrogel can be modulated by external stimuli, thereby further generating a distinct electrical signal, which was suitable for strain sensing application.[7] Generally, the mechanical property of traditional conductive hydrogels was improved by the covalently bonded polymer network via the introduction of chemical crosslinkers. Unfortunately, they will lead to low chain fluidity and brittleness caused by poor energy dissipation,[8] which significantly restricts their practical utilization. To address these limitations, many researchers have devoted themselves to developing physical crosslinking hydrogel networks based on supramolecular interactions, such as hydrogen bonding, ionic bonding, and metal coordination.[9−12] These reversible noncovalent bonds can be dissociated and reorganized under applied stress, facilitating enhanced energy dissipation and self-healing performance. The crucial factor enables the hydrogel to withstand greater deformation, meeting the flexibility requirements of wearable devices. Also, the use of toxic initiators and time-consuming processes in the preparation of hydrogel-based sensors poses a severe challenge for widespread application. Recently, our group has developed several efficient green preparation strategies, but molecular-level signal detection is still difficult, thereby impairing their potential for multiple scenarios.[13,14]

Abnormal ion concentrations in sweat are related to various health situations, including Minamata disease, anemia, osteoporosis, and Welsh disease.[15,16] They can be measured by using atomic absorption spectrometry (AAS) or inductively coupled plasma− mass spectrometry (ICP−MS).[17,18] These techniques need expensive equipment and a complex procedure, making them inappropriate for noninvasive early-stage health monitoring. To realize portable and in situ ion detection, optical sensing methods have attracted much attention because of their low cost, high sensitivity, and strong selectivity. By integrating fluorescent material into a polymer matrix, researchers have exploited diverse fluorescent sensors

Received: July 20, 2025
Revised: November 4, 2025
Accepted: November 10, 2025
Published: November 19, 2025

https://doi.org/10.1021/acs.analchem.5c04212
Anal. Chem. 2025, 97, 25937−25945

Scheme 1. Schematic Process for the Preparation of the SHTP Hydrogel

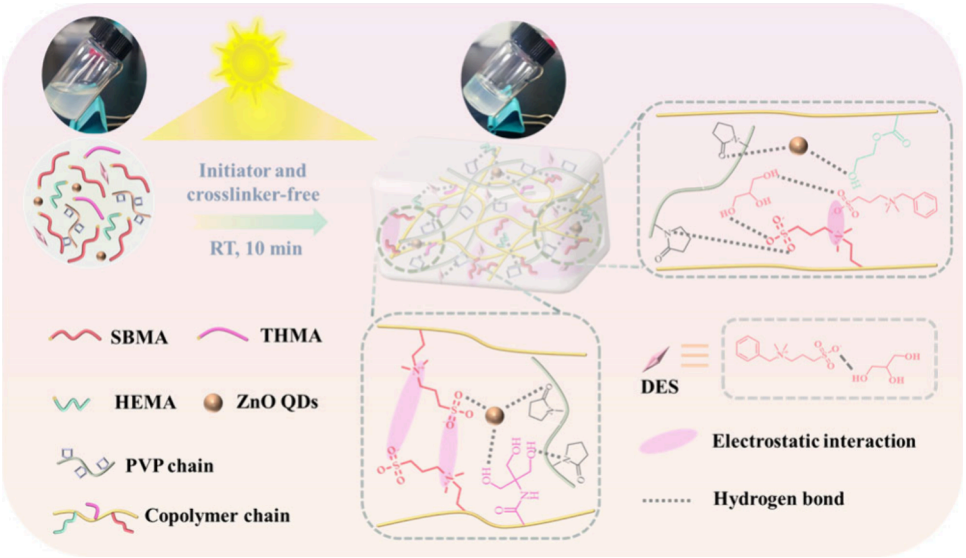

for responding to ions. For example, Qiu et al. fabricated surface-patterned fluorescent hydrogel sensors based on traditional Chinese medicine (TCM)-derived carbon dots (CDs) to quantitatively detect trace Fe^{3+} in complex samples.[19] Chen and co-workers synthesized a series of luminescent glycopolymers which were constructed from a nonaromatic sugar monomer and methacrylic acid, and they have been demonstrated to selectively monitor the concentrations of certain metal ions.[20] Guo et al. prepared a novel radiometric fluorescence sensor with graphitic carbon nitride nanoparticles (CNNPs) and cadmium telluride sulfide ($CdTe_{0.16}S_{0.84}$) QDs, which can realize portable on-site analysis of trace mercury ions.[18] Compared to the above fluorescent materials, ZnO QDs exhibit lower toxicity, better photostability, and mild synthesis conditions, providing an ideal choice for visual ion detection.[21,22]

In this study, a novel noncovalent cross-linked multifunctional hydrogel sensor was constructed by adopting an efficient green strategy. From [2-(methylacryloyloxy)ethyl]dimethyl-(3-sulpropyl) (SBMA), 2-hydroxyethyl methacrylate (HEMA), N-[tris (hydroxymethyl)methyl]acrylamide (THMA), polyvinylpyrrolidone (PVP), and ZnO QDs via a DES-catalyzed sunlight-induced system (Scheme 1), the P(SBMA-*co*-HEMA-*co*-THMA)/PVP IPN hydrogel (SHTP) can be obtained by an initiator and cross-linker-free process within 10 min. It demonstrates excellent transparency, favorable mechanical properties, and reliable adhesion. Based on the intrinsic ionic conductivity and fluorescence response characteristics of the SHTP hydrogel, it can achieve a quantitative detection of ions and the real-time monitoring of external stress. This design concept conforms to the sustainable green development principle of multifunctional wearable devices.

EXPERIMENTAL SECTION

Materials. SBMA (≥98%) was purchased from Bide Pharmtech Co., Ltd. N,N-Dimethylbenzylamine (98%), HEMA, 1,3-propanesultone (99%), $Zn(Ac)_2{\cdot}2H_2O$ (99%), 3-aminopropyltriethoxysilane (APTES, 98%), and PVP (M_n = 8000 g/mol) were obtained from Aladdin. THMA was obtained from Maclin Biochemical Technology Co. Ltd. Deionized water (DI, resistivity = 18.2 MΩ·cm) was purified using a Millipore filtration system prior to use. All other chemical reagents were procured from commercial sources and employed without additional purification.

Preparation of 3-(Benzyldimethylammonio)propane-1-sulfonate (SP). 3-(Benzyldimethylammonio)propane-1-sulfonate was synthesized according to previous work.[14] In brief, 1,3-propanesultone (0.285 mol, 25 mL) dispersed in an equal volume of ethyl acetate was maintained at 50 °C under continuous magnetic agitation. Then, a mixture of N,N-dimethylbenzylamine (0.285 mol, 42.8 mL) in ethyl acetate (25 mL) was poured into it. Meanwhile, a certain amount of solvent should be used to avoid the adverse consequences of overheating. The crude product can be harvested within a few minutes, followed by washing, centrifuging, and drying to obtain the pure white solid product.

Preparation of Water-Soluble ZnO NPs. Water-soluble ZnO NPs were synthesized in a reported work.[23] First, 2.64 g (12 mmol) of $Zn(Ac)_2{\cdot}2H_2O$ was dispersed in anhydrous ethanol solution (120 mL) and refluxed for 3 h at 80 °C. Next, a solution of 0.94 g (16.8 mmol) of KOH in 20 mL of ethanol was added dropwise to the above solution, followed by continuous stirring until the colorless and clear mixture was formed. Afterward, 256 μL of APTES and 5 mL of deionized water were introduced into the obtained ZnO QDs solution and then stirred at RT for 8 h. In the end, the pale-yellow products were collected by precipitating, centrifuging, and drying.

Preparation of DES (SP-Gly). 3-(Benzyldimethylammonio)propane-1-sulfonate and glycerol were mixed in a molar ratio of 1:4 and then stirred at 80 °C for 2 h to obtain a transparent and homogeneous liquid, which was coded as SP-Gly.[14]

Preparation of SHTP Hydrogels. The as-prepared hydrogels were constructed by a sunlight (73.6 mW/cm^2)-driven self-polymerization system, eliminating the dependence on chemical cross-linkers and initiators. In brief, SBMA, THMA, HEMA, PVP, DES, and ZnO QDs were mixed with deionized water under room temperature (RT). The resulting homogeneous solution was then processed into the transparent hydrogel strip (length = 60 mm, width = 20 mm, thickness = 20 mm) after 10 min of exposure to sunlight at RT.

https://doi.org/10.1021/acs.analchem.5c04212
Anal. Chem. 2025, 97, 25937−25945

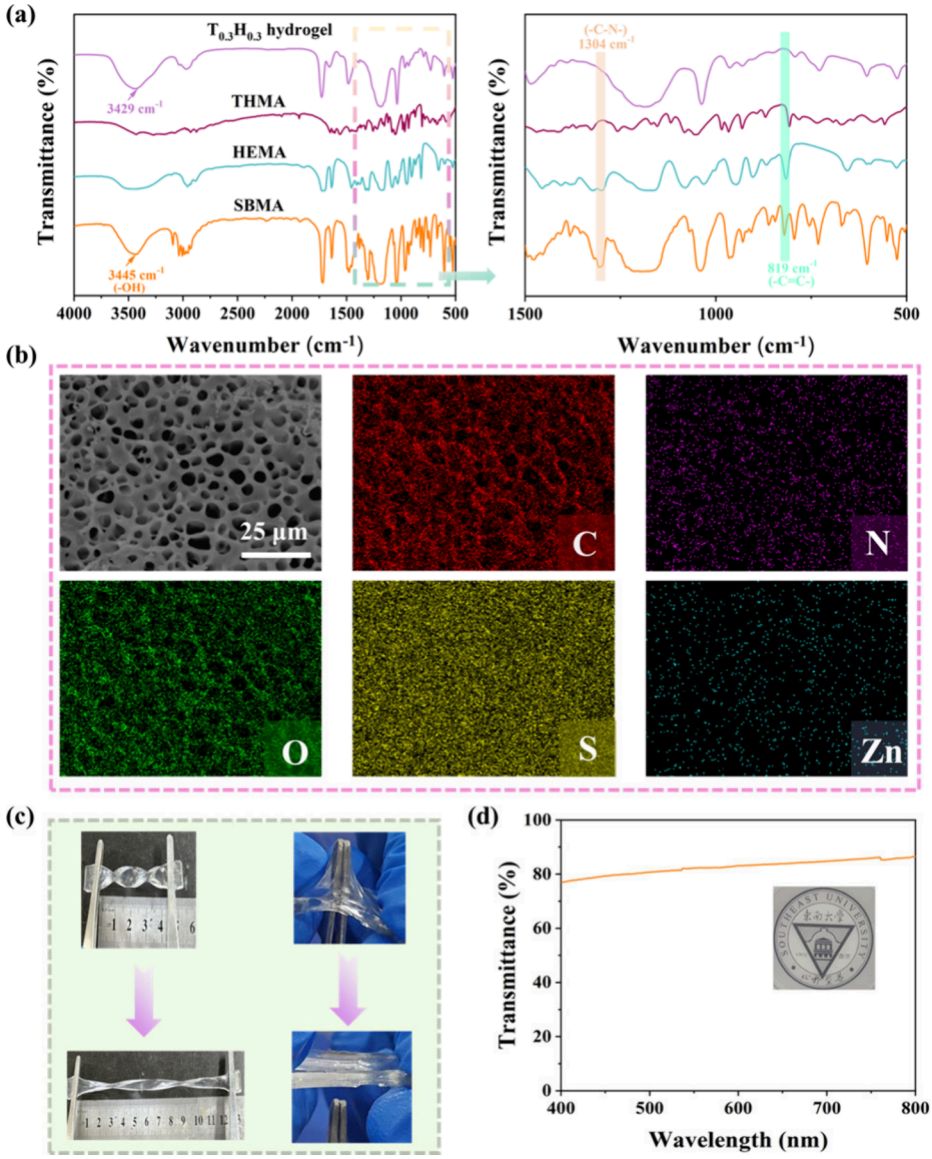

Figure 1. (a) FT-IR spectra of SBMA, HEMA, the THMA monomer, and the $T_{0.3}H_{0.3}$ hydrogel. (b) SEM image and related elemental mapping of the $T_{0.3}H_{0.3}$ hydrogel. (c) Photographs of the $T_{0.3}H_{0.3}$ hydrogel treated by stretching in the twisted state and anti-pricking behavior. (d) UV−vis transmittance of the $T_{0.3}H_{0.3}$ hydrogel (inset photograph showing the background logo under the $T_{0.3}H_{0.3}$ hydrogel).

General Characterization. The internal microstructure and element content of hydrogels were determined with a scanning electron microscope (SEM, FEI Sirion) at an acceleration voltage of 15 kV equipped with an energy-dispersive spectrometer (EDS). The morphology of nanoparticles was confirmed by transmission electron microscopy (TEM, Talos F200X). X-ray diffraction (XRD) data were collected with an Ultima IV X-ray diffractometer (Rigaku Corporation, Japan) with Cu Kα radiation in the region of 2θ from 20 to 80°. Fourier transform infrared (FT-IR, Nicolet iS10) spectra in the range of 500−4000 cm^{-1} to verify the chemical structure of hydrogels were obtained using the potassium bromide tableting method. The fluorescence emission spectra of all samples were measured on a Shimadzu RF-6000 with an excitation wavelength of 365 nm. UV−vis spectroscopy was recorded on a UV-2600 spectrophotometer (Shimadzu) ranging from 400 to 800 nm. The conductivity of hydrogels was characterized by a digital four-probe tester (RTS-9, 4-probe tech).

Mechanical Test. The mechanical performance of hydrogel samples was determined by an electronic universal testing machine (MTS Exceed E43) using a 50 N load cell. The speed of tensile tests was conducted at 50 mm/min. As for compression tests, the cylindrical hydrogel samples (height = 20 mm, diameter = 15 mm) were used at a rate of 8 mm/min. Young's modulus was obtained from the slope of the strain curve from 5 to 20%. Toughness data were calculated from the region under a stress−strain curve. In addition, the dissipated energy was the integral area of the tensile cycle curve.

Adhesion Tests. The $T_{0.3}H_{0.3}$ hydrogel was adhered to the middle of two identical substrates, containing paper, glass, polytetrafluoroethylene (PTFE), copper, and polyethylene terephthalate (PET), with a joint zone of 10 mm × 20 mm. Then, the hydrogel was peeled away from the substrates at a speed of 50 mm/min. The adhesion strength was determined by eq 1

https://doi.org/10.1021/acs.analchem.5c04212
Anal. Chem. 2025, 97, 25937−25945

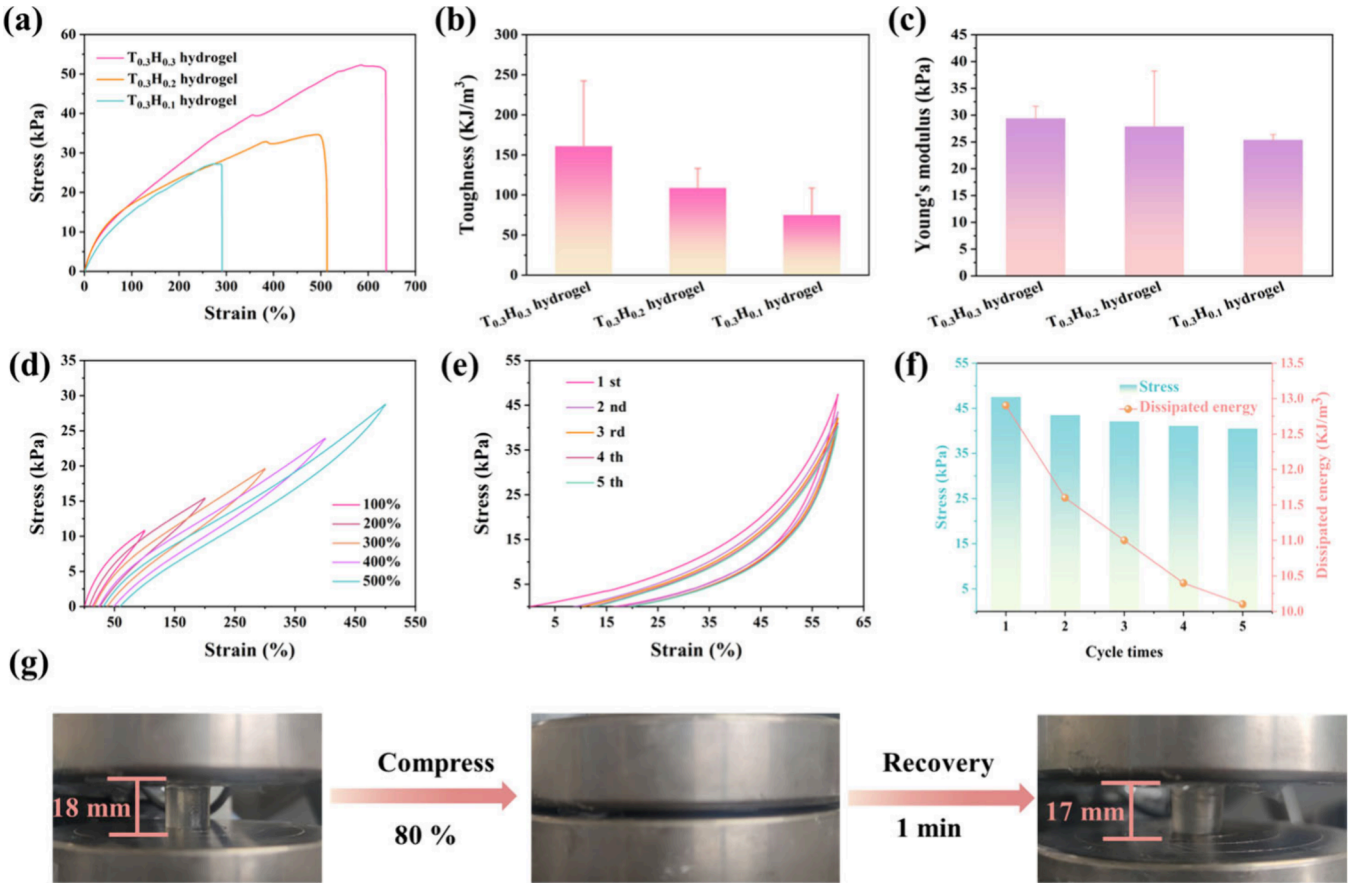

Figure 2. (a) Tensile stress−strain curves of diverse SHTP hydrogels. (b) Toughness. (c) Young's modulus of the as-prepared hydrogels. (d) Cyclic tensile tests of the $T_{0.3}H_{0.3}$ hydrogel under 100, 200, 300, 400 and 500% strain. (e) Five successive compression cycles of the $T_{0.3}H_{0.3}$ hydrogel at 60% strain. (f) Compression stress and dissipated energy of the $T_{0.3}H_{0.3}$ hydrogel during the five compression cycles. (g) Elastic performance of the $T_{0.3}H_{0.3}$ hydrogel after compressing to 80% strain.

$$P = F_{max}/S \quad (1)$$

where F_{max} is the peak force generated during the separation of the hydrogel and substrate and S is the initial overlapping zone.

Electrical Sensing Tests. To construct a hydrogel-based sensor, both ends of the as-prepared $T_{0.3}H_{0.3}$ hydrogel sample (width = 5 mm, length = 30 mm, and thickness = 4 mm) were attached by copper foil tape and connected to external wires. Furthermore, the sensor was then mounted on a digital multimeter (Keysight 34461A, America) and subjected to repeated stretching at various strains. The variation in relative resistance was calculated with formula 2

$$\Delta R/R_0 = (R - R_0)/R_0 \times 100\% \quad (2)$$

where R_0 is the original resistance of the hydrogel without strain and R is the resistance during the deformation period.

The gauge factor (GF) was computed with formula 3

$$GF = (\Delta R/R_0)/\varepsilon \quad (3)$$

where ε is the strain applied throughout the test.

RESULTS AND DISCUSSION

Characterization of the SHTP Hydrogel. The SHTP hydrogel comprised of different components was prepared by an initiator and crosslinker-free method. They are named T_xH_y hydrogels, where x and y represent the relevant added amount (g) of THMA and volume (mL) of HEMA (Table S1). During the polymerization process, the SBMA monomer at high concentration was first photoactivated by sunlight to produce free radicals and then copolymerized with HEMA and THMA, the noncovalent crosslinking was achieved by electrostatic interaction and hydrogen bonding among the inner polymer network. The addition of PVP acted as a second network to form an IPN structure in one pot, providing more impressive mechanical properties of the hydrogel. Furthermore, DES not only affords extra free ions to enhance the inherent conductivity of the hydrogel but also plays a great role in reducing the gelation time due to its high-viscosity effect.[14,24] The doped ZnO QDs can also serve as a physical bonding site via the amino group on their surface, enhancing the overall mechanical performance of the polymer network by increasing the crosslinking density. Meanwhile, its unique optoelectronic characteristic endows the SHTP hydrogel with molecular-level detection capacity.

The uniform quasi-spherical structure of 4.6 ± 0.2 nm synthetic ZnO QDs was determined by the high-resolution (HR) TEM result, moreover, the selected area electron diffraction (SAED) revealed their polycrystalline structure, with the interplanar spacing at 0.11 and 0.16 nm, consistent with the characteristic (203) and (101) facets of pure ZnO, respectively (Figure S1a−c). As shown in Figure S1d, the XRD pattern could be ascribed to the hexagonal crystal phase of

https://doi.org/10.1021/acs.analchem.5c04212
Anal. Chem. 2025, 97, 25937−25945

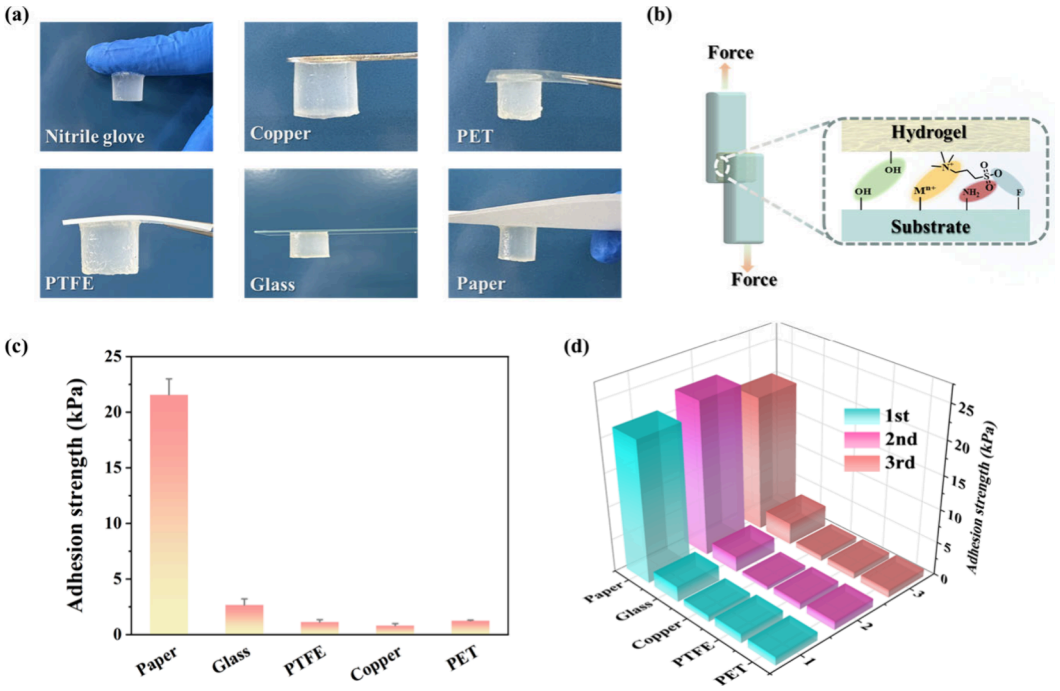

Figure 3. (a) Pictures of the $T_{0.3}H_{0.3}$ hydrogel adhered to different substrates. (b) Diagram of adhesion test and probable adhesive mechanism between the hydrogel and substrate. (c) Adhesion strength of the $T_{0.3}H_{0.3}$ hydrogel toward substrates. (d) Cyclic adhesion behavior of the $T_{0.3}H_{0.3}$ hydrogel.

ZnO (PDF no. 89-1397). Taking the $T_{0.3}H_{0.3}$ hydrogel as the typical sample, the chemical structure of the SHTP hydrogel was demonstrated by FT-IR spectroscopy, and the characteristic peak at 819 cm^{-1} belonging to the −C═C− twisting vibration vanished after the polymerization driven by sunlight,[13] indicating the successful copolymerization of SBMA, HEMA, and THMA monomers. Meanwhile, the representative peak for the −OH stretching vibration was shifted from 3445 to 3429 cm^{-1} because of the hydrogen bond interaction in the inner polymer network,[25] accompanied by the disappearance of the peak at 1304 cm^{-1} assigned to the −C−N− group resulting from the electrostatic interaction between the $-N^+(CH_3)_2-$ and $-SO_3-$ groups[26] (Figure 1a), which revealed the fundamental mechanism for the formation of the SHTP hydrogel. It can be observed from SEM and corresponding element mapping results that the $T_{0.3}H_{0.3}$ hydrogel possessed a three-dimensional porous structure with a uniform distribution of C, N, O, S, and Zn elements (Figure 1b), which was beneficial for ion transportation.[27] Moreover, it was found to have admirable mechanical and optical performance, as shown in Figure 1c, and the $T_{0.3}H_{0.3}$ hydrogel could be highly stretched even in a twisted, knotted (Figure S2) state and could withstand extreme puncturing. Additionally, the resulting hydrogel exhibited favorable transparency with a transmittance of around 80% in the visible wavelength region from 400 to 800 nm. As depicted in the inset of Figure 1d, the background logo was distinctly seen beneath the $T_{0.3}H_{0.3}$ hydrogel.

Mechanical Property of the SHTP Hydrogel. It is imperative that flexible hydrogel-based wearable sensors exhibit good mechanical properties. To evaluate the mechanical performance of the SHTP hydrogel, we conducted a sequence of tensile and compression tests. As shown in Figure 2a−c, the as-prepared SHTP hydrogel exhibited enhanced fracture strength (from 27.2 to 51.0 kPa), breaking elongation (from 291 to 636%), Young's modulus (from 25.4 to 29.4 kPa), and toughness (from 75.1 to 160.9 KJ/m^3) as HEMA increased, which could be ascribed to the more efficient hydrogen bond effects. Owing to the non-covalent crosslinking effect in the polymer network, including hydrogen bond and electrostatic interaction, the $T_{0.3}H_{0.3}$ hydrogel had an excellent dissipation capacity, which displayed rapid resilience even close to the limit of breaking elongation (Movie S1) and withstood a maximum weight of up to 272 g (Figure S3). To quantifiably assess the dissipation and elasticity performance on SHTP hydrogels suffering from the recovery of non-covalent bonds, we chose the $T_{0.3}H_{0.3}$ hydrogel as a typical sample to conduct cyclic tensile and compressive tests. It should be noted that the hysteresis loop within the stress−strain curve of the $T_{0.3}H_{0.3}$ hydrogel remained in the strain in the region from 100 to 500% (Figure 2d), demonstrating its exceptional resilient recovery (Table S2), and the relevant dissipated energy was augmented from 12.0 to 131.4 KJ/m^3 (Figure S4). Furthermore, five-cycle loading−unloading compressive tests under 60% strain were conducted to assess its fatigue resistance. As shown in Figure 2e-f, the compressive stress and dissipated energy of the hydrogel slightly decreased after the first cycle and then tended to be stable. The low value of the compressive dissipated energy of the $T_{0.3}H_{0.3}$ hydrogel during cyclic measurement (Table S3) means that the majority of the energy is stored as elastic potential energy rather than being lost as thermal energy. This serves as the driving force for the material to return to its original state, resulting in its excellent elastic performance. Moreover, the $T_{0.3}H_{0.3}$ hydrogel can also withstand 80% compressive strain and almost recover to its pristine shape quickly, benefiting from the reversible construction of non-covalent bonds (Figure 2g).

Adhesive Performance of the SHTP Hydrogel. Interface resistance between a wearable sensor and skin will be generated by the failure to fit tightly between them,

https://doi.org/10.1021/acs.analchem.5c04212
Anal. Chem. 2025, 97, 25937−25945

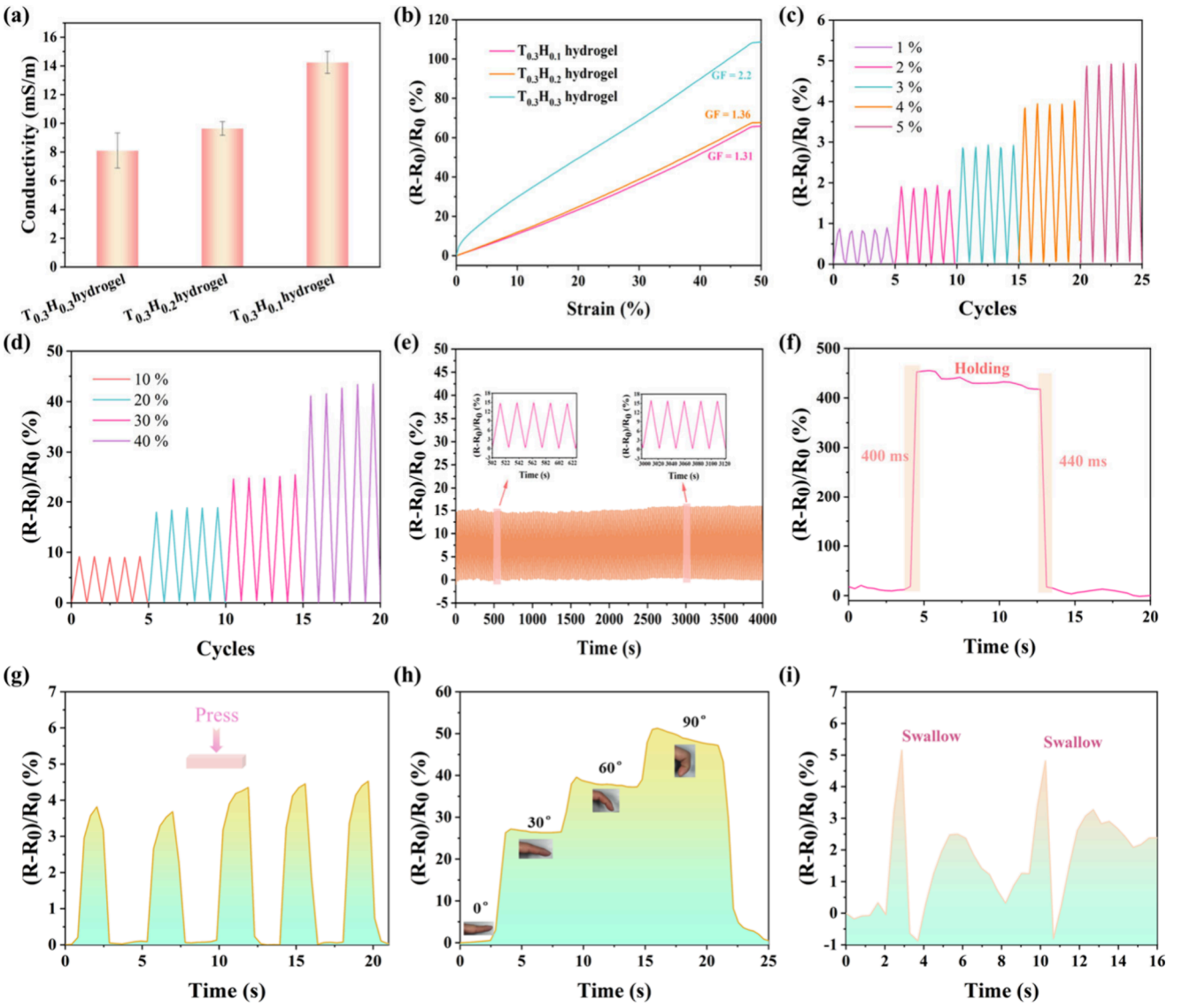

Figure 4. (a) Conductivity of SHTP hydrogels. (b) Tunable GF value of the SHTP hydrogel at strain ranging from 0 to 50%. Real-time relative resistance monitored at changed tensile strains of (c) 1−5% and (d) 10−40%. (e) Long-term stability examination of a $T_{0.3}H_{0.3}$ hydrogel-based sensor exerted by 10% tensile strain for 150 cycles. (f) Response time of $T_{0.3}H_{0.3}$ hydrogel-based sensors. Real-time relative resistance variation of the $T_{0.3}H_{0.3}$ hydrogel-based sensor replying to (g) press and (h) finger bending at diverse angles (0, 30, 60, and 90°). (i) Swallow.

significantly weakening the detection accuracy of sensors for external stimuli, which can be overcome by their instinctive reliable adhesion ability. It was noted that the $T_{0.3}H_{0.3}$ hydrogel exhibited admirable adhesion to human skin (Figure S5) and other different materials, such as nitrile glove, copper, PET, PTFE, glass, and paper, and the adhesion mechanism can be attributed to the synergistic function among the electrostatic interaction, hydrogen bond, dipole−dipole interaction, and metal coordination on the surfaces of the hydrogel and material (Figure 3a−3b).[13] To assess the adhesion performance of the as-prepared hydrogel, a lap-shear test was adopted to verify the adhesion strength toward different substrates. As depicted in Figure 3c, the maximum adhesion strength of the $T_{0.3}H_{0.3}$ hydrogel on paper (21.6 kPa) was much higher than that on other substrates, whereas the corresponding adhesion strengths on glass, PTFE, copper, and PET were 2.6, 1.1, 0.8, and 1.2 kPa, respectively. This phenomenon could be explained by the fact that the hydrogen bond interaction was significantly enhanced due to the abundant hydroxyl groups within paper. Additionally, the results of the cyclic adhesion experiment revealed that the maximum adhesion strength of the $T_{0.3}H_{0.3}$ hydrogel to diverse substrates remained relatively stable over three adhesion−peel cycles, proving its reliable adhesion capacity (Figure 3d).

Sensing Performance of the SHTP Hydrogel. The existence of zwitterionic groups leads to the inherent ionic conductivity, thereby endowing as-prepared hydrogels with electric sensing properties responsive to external stimuli, which enables them to be suitable for wearable sensors. With the increasing addition of HEMA content, the conductivity of resulting hydrogels decreased from 14.3 to 8.1 mS/m (Figure 4a). On the contrary, the gauge factor (GF), denoted as the ratio of relative resistance change ($(R\text{-}R_0)/R_0$),[28] which reflects an indicative parameter for sensitivity of hydrogel-based sensors was increased from 1.31 to 2.2 in the daily human physiological strain region of 0−40% (Figure 4b), it can be assigned to reason that the higher conductivity will impair ionic transfer resistance to a certain extent. Moreover, we also

https://doi.org/10.1021/acs.analchem.5c04212
Anal. Chem. 2025, 97, 25937−25945

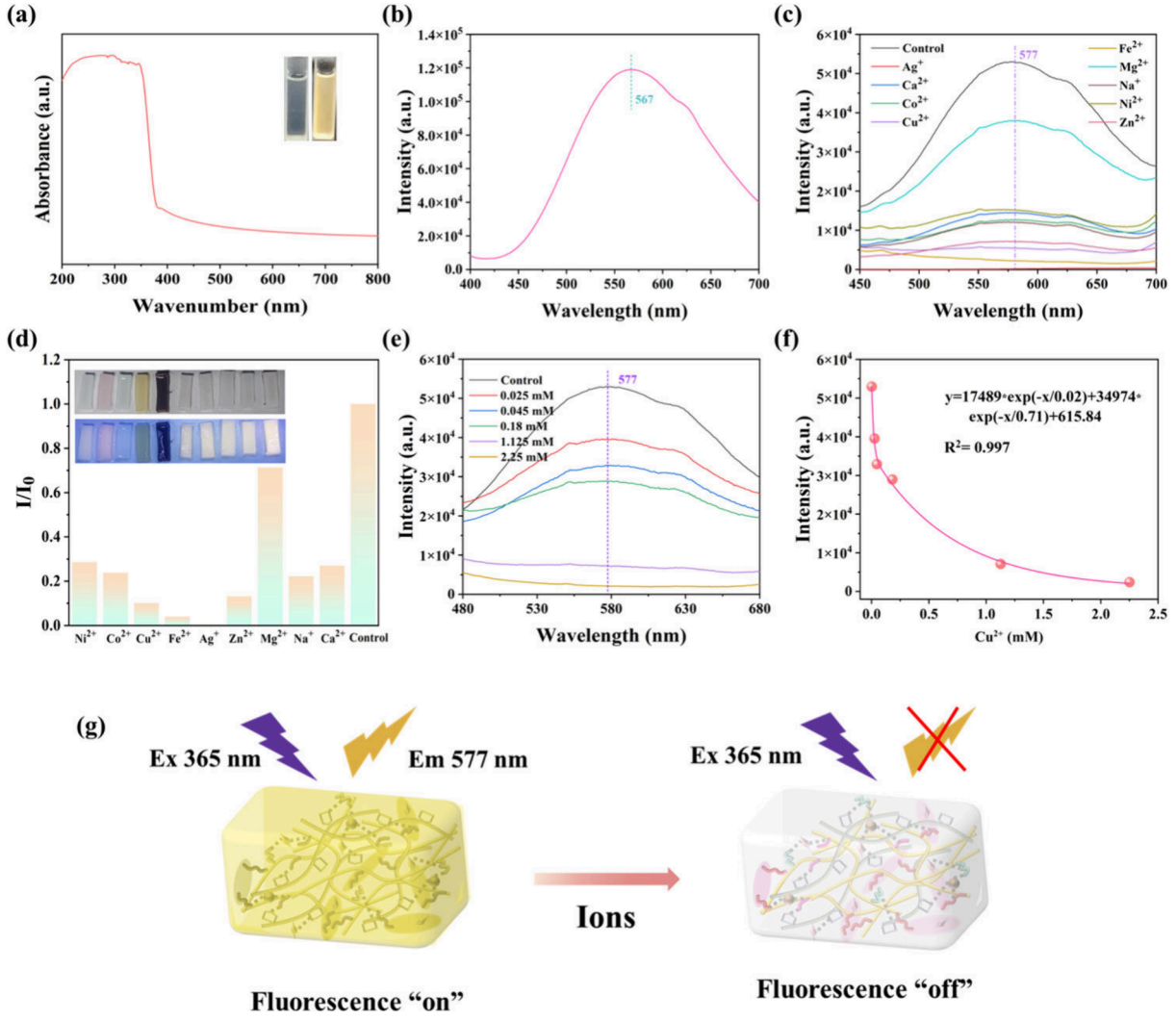

Figure 5. (a) UV−vis absorption spectra of ZnO QDs solution. (Inset: optical picture of it under a 365 nm UV lamp.) (b) Emission fluorescence spectrum of the ZnO QDs solution. (c) Emission fluorescence spectra of the $T_{0.3}H_{0.3}$ hydrogel after treatment with different ions. (d) Maximal fluorescence intensity ratio of the $T_{0.3}H_{0.3}$ hydrogel after combination with diverse ions (18 mM) at 577 nm. (Inset: corresponding photographs of the $T_{0.3}H_{0.3}$ hydrogel at 365 nm excitation and visible light (from left to right: Ni^{2+}, Co^{2+}, Cu^{2+}, Fe^{2+}, Ag^{+}, Zn^{2+}, Mg^{2+}, Na^{+}, Ca^{2+}, blank). (e) Emission fluorescence spectra of the $T_{0.3}H_{0.3}$ hydrogel after treatment with copper ions at different concentrations. (f) Related fitting curve and equation of emission fluorescence intensity. (g) Schematic illustration of fluorescence quenching caused by the interaction between the as-prepared hydrogel and ions.

chose $T_{0.3}H_{0.3}$ hydrogel as a typical illustrative sample to verify its prospects for wearable sensors. It was found that $T_{0.3}H_{0.3}$ hydrogel-based sensor can generate a stable signal output when applied small (1%−5%) and even large (10%−40%) stimuli in each five cycles, meeting the requirement for human motion daily use (Figure 4c-4d). Besides, the change of relative resistance still endured constant over 150 cycles at 10% strain, demonstrating the consistent long-term cyclic sensing performance of the as-prepared $T_{0.3}H_{0.3}$ hydrogel (Figure 4e). The resulting hydrogel suffered from rapid response times during the stretching (400 ms) and recovery (440 ms) process, ensuring its real-time signal detection when subjected to external stimuli (Figure 4f). External pressure will cause a change in the cross-section of hydrogel-based sensors, further altering the inner ion transport channel of the polymer network within the hydrogel, thus the related pressure could be accurately detected (Figure 4g). Moreover, as shown in Figure 4h−4i, other physical motions including diverse bending angles (30, 60, and 90°) of the finger joint and the swallowing process could also be monitored in real time by attachment to a particular area for on-demand detection.

Ionic Determination Capacity of the SHTP Hydrogel. The photoresponsive characteristic component is crucial for the as-prepared hydrogel to realize ionic detection, which will undergo a quenching process through fluorescence resonance energy transfer when combined with ions.[29] Therefore, we tested the optical property of ZnO QDs, and it was found that the aqueous ZnO QDs solution exhibited bright-yellow fluorescence when excited by UV light at 365 nm (inset of Figure 5a). As illustrated in Figure 5a−5b, the UV−vis and fluorescence spectroscopy showed a broad absorption band ranging from 200 to 378 nm and a fluorescence emission wavelength of 567 nm, which was caused by the intrinsic band gap absorption of ZnO QDs owing to the electron transition between valence and conduction bands.[30] To further validate the selectivity of the ion detection capacity based on the SHTP hydrogel as a fluorescent probe, nine kinds of metal ions including Ag^{+}, Ca^{2+}, Co^{2+}, Cu^{2+}, Fe^{2+}, Mg^{2+}, Na^{+}, Ni^{2+}, and

https://doi.org/10.1021/acs.analchem.5c04212
Anal. Chem. 2025, 97, 25937−25945

Zn^{2+} at 18 mM were incubated with the $T_{0.3}H_{0.3}$ hydrogel several times and then the related fluorescence emission spectra of the hydrogel were characterized. As evidenced in Figure 5c−5d, the fluorescence intensity of the hydrogel declined in different contents, proving the excellent ion selectivity of the hydrogel, which demonstrates its potential application in the early diagnosis of abnormal ions caused by certain diseases. It should be noted that the observed emission wavelength of the $T_{0.3}H_{0.3}$ hydrogel was increased from 567 to 577 nm. This phenomenon can be explained by the interaction between the hydrogel matrix and excited-state ZnO QDs, resulting in energy relaxation. The quantitative ion detection performance of hydrogels was evaluated by adding standard Cu^{2+} solution with different concentrations. It should be noted that the fluorescence intensity decreased with the increase in Cu^{2+} concentration, and the obtained detection limit was 0.025 mM (Figure 5e). In addition, the correlation intensity values could be fitted to the nonlinearity analyzed by the statistical model of a Gaussian function (R^2 = 0.997, Figure 5f) according to the quenching process of interaction between hydrogels and ions (Figure 5g), satisfying the requirement for the accurate detection of ions.

CONCLUSIONS

In brief, we utilized an efficient green method to construct a new type of physical crosslinked IPN hydrogel, which was prepared within 10 min by the DES-catalyzed sunlight-induced polymerization without any use of initiator and chemical crosslinker. It was determined that the as-prepared SHTP hydrogels doped with ZnO QDs possessed favorable transparency (∼80%), admirable extensibility (up to 636%), excellent elastic properties, and reliable adhesion capacity. Given the instinct conductivity of SHTP hydrogels, they were suitable to serve as wearable sensors for real-time physiological motion detection, such as different strains, finger bending from 0 to 90°, and swallow behavior. The rapid response time (400 ms) and stable signal output during long-term (350 cycles) testing ensure their potential wearable sensing application in daily life. In addition, they can also be applied in quantitatively monitoring the concentration of ions based on the fluorescence resonance energy transfer effect, which makes them excellent candidates for diagnosing certain diseases in the early period due to the abnormal ions. We believe that our contribution broadened a prospective avenue for innovative multifunctional wearable electronics.

ASSOCIATED CONTENT

Supporting Information

The Supporting Information is available free of charge at https://pubs.acs.org/doi/10.1021/acs.analchem.5c04212.

Additional tables and figures as mentioned in the manuscript (PDF)

Stretching and rebounding process of the $T_{0.3}H_{0.3}$ hydrogel (Movie S1) (MP4)

AUTHOR INFORMATION

Corresponding Authors

Michael Daramola − *Department of Chemical Engineering, University of Pretoria, Pretoria 0002, South Africa*; Email: michael.daramola@up.ac.za

Guodong Fu − *School of Chemistry and Chemical Engineering, Southeast University, Nanjing 211189, P. R. China*; orcid.org/0000-0001-7571-9675; Email: fu7352@seu.edu.cn

Authors

Jun Hu − *School of Chemistry and Chemical Engineering, Southeast University, Nanjing 211189, P. R. China*

Yuting Tian − *School of Chemistry and Chemical Engineering, Southeast University, Nanjing 211189, P. R. China*

Xiaoying Xin − *School of Chemistry and Chemical Engineering, Southeast University, Nanjing 211189, P. R. China*

Complete contact information is available at: https://pubs.acs.org/10.1021/acs.analchem.5c04212

Author Contributions

J.H.: Conceptualization, methodology, investigation, data curation, and writing−original draft. Y.T.: Investigation and data curation. X.X.: Investigation and data curation. M.D.: Review and editing. G.F.: Funding acquisition, supervision.

Notes

The authors declare no competing financial interest.

ACKNOWLEDGMENTS

This work was funded by the National Natural Science Foundation of China (No. 52073059) and Basic Research Program of Jiangsu (No. BK20252005).

REFERENCES

(1) Xu, C.; Wang, Y.; Zhang, J.; Wan, J.; Xiang, Z.; Nie, Z.; Xu, J.; Lin, X.; Zhao, P.; Wang, Y.; Zhang, S.; Zhang, J.; Liu, C.; Xue, N.; Zhao, W.; Han, M. *Sci. Adv.* **2024**, *10*, No. eadp6094.

(2) Cai, X.; Wang, X.; Bian, F.; Li, J.; Zhou, R.; Hu, J.; Lin, S. *Chem. Eng. J.* **2024**, *498*, No. 154934.

(3) Gao, X.; Wu, J.; Wang, Y.; Wang, Y.; Zhang, Y.; Nguyen, T. T.; Guo, M. *Int. J. Biol. Macromol.* **2024**, *265*, No. 131118.

(4) Wang, R.; Qiu, T.; Zhang, Y.; Rein, M.; Stolyarov, A.; Zhang, J.; Seidel, G. D.; Johnson, B. N.; Wang, A.; Jia, X. *Adv. Funct. Mater.* **2024**, *34* (40), No. 2403918.

(5) Li, M.; Chen, D.; Sun, X.; Xu, Z.; Yang, Y.; Song, Y.; Jiang, F. *Carbohydr. Polym.* **2022**, *284*, No. 119199.

(6) Qin, Z.; Li, Y.; Wang, X.; Liu, Y.; Li, N.; Xu, Q.; Ye, L.; Jiao, T. *J. Mater. Chem. A* **2024**, *12* (18), 10808−10818.

(7) Li, R.; Ren, J.; Zhang, M.; Li, M.; Li, Y.; Yang, W. *Biomacromolecules* **2024**, *25* (2), 614−625.

(8) Cui, B.; Guo, C.; Zhang, Z.; Fu, G. *Chem. Eng. J.* **2023**, *455*, No. 140822.

(9) Xu, A.; Sun, T.; Liu, R.; Li, L.; Gong, Y.; Xiao, Z. *Green Chem.* **2024**, *26* (7), 3926−3939.

(10) Qi, M.; Yang, R.; Wang, Z.; Liu, Y.; Zhang, Q.; He, B.; Li, K.; Yang, Q.; Wei, L.; Pan, C.; Chen, M. *Adv. Funct. Mater.* **2023**, *33* (17), No. 2214479.

(11) Cui, S.; Zhang, S.; Zhang, F.; Lin, R.; Tang, C.; Jing, X. *Carbohydr. Polym.* **2024**, *323*, No. 121385.

(12) Zou, X.; Wang, X.; Bai, Z.; Yue, O.; Wei, C.; Xie, L.; Zhang, H.; Liu, X. *Chem. Eng. J.* **2023**, *463*, No. 142349.

(13) Hu, J.; Guo, J.; Zhao, J.; Chen, Z.; Kalulu, M.; Chen, G.; Fu, G. *ACS Appl. Mater. Interfaces* **2024**, *16* (8), 10671−10681.

(14) Hu, J.; Shan, F.; Tian, Y.; Wei, J.; Chen, Z.; Liu, W.; Chen, G.; Fu, G. *Chem. Eng. J.* **2025**, *504*, No. 158837.

(15) Xu, T.; Zhang, X.; Yang, H.; Li, H.; Zhang, S.; Yang, Z.; Jia, X.; Liu, X.; Li, J. *Chem. Eng. J.* **2023**, *467*, No. 143465.

(16) Gao, W.; Nyein, H. Y. Y.; Shahpar, Z.; Fahad, H. M.; Chen, K.; Emaminejad, S.; Gao, Y.; Tai, L.-C.; Ota, H.; Wu, E.; Bullock, J.; Zeng, Y.; Lien, D.-H.; Javey, A. *ACS Sens.* **2016**, *1* (7), 866−874.

(17) Xu, J.; Guo, Y.; Gong, T.; Cui, K.; Hou, L.; Yuan, C. *Inorg. Chem. Commun.* **2022**, *145*, No. 110047.

(18) Guo, X.; Xiao, J.; Zhang, Y.; Zhang, Q.; Yang, J.; Wei, Y.; Wang, L.; Yao, W. *Sens. Actuators B Chem.* **2024**, *413*, No. 135846.
(19) Qiu, Y.; Xia, L.; Shi, R.; Yuan, L.; Zhang, Y.; Chen, A.; Zhou, K.; Wu, H.; Zhang, K.; Xia, Z.; Fu, Q. *Sens. Actuators B Chem.* **2024**, *401*, No. 134958.
(20) Hu, J.; Lu, K.; Gu, C.; Heng, X.; Shan, F.; Chen, G. *Biomacromolecules* **2022**, *23* (3), 1075−1082.
(21) Zhang, M.; Qiao, X.; Han, W.; Jiang, T.; Liu, F.; Zhao, X. *Carbohydr. Polym.* **2021**, *266*, No. 118100.
(22) Guo, Y.; Zhang, Y.; Li, T.; Tao, T. *J. Environ. Chem. Eng.* **2021**, *9* (6), No. 106800.
(23) Chen, N.; Yong, W.-X.; Xiong, T.-D.; Fu, G.-D. *J. Mater. Chem. C* **2023**, *11* (28), 9570−9577.
(24) Liu, Y.-X.; Bian, C.; Zhou, Y.-N.; Li, J.-J.; Luo, Z.-H. *Ind. Eng. Chem. Res.* **2020**, *59* (31), 13870−13878.
(25) Wang, N.; Tian, J.; Janaswamy, S.; Cao, G.; Teng, W.; Song, S.; Wen, C. *Int. J. Biol. Macromol.* **2023**, *242*, No. 124763.
(26) Huang, X.; Chen, C.; Ma, X.; Zhu, T.; Ma, W.; Jin, Q.; Du, R.; Cai, Y.; Zhang, M.; Kong, D.; Wang, M.; Ren, J.; Zhang, Q.; Jia, X. *Adv. Funct. Mater.* **2023**, *33* (38), No. 2302846.
(27) Li, Y.; Wen, X.; Li, X.; Zahid, M.; Wang, H.; Zhang, J. *Carbohydr. Polym.* **2025**, *348*, No. 122858.
(28) Zhu, T.; Ni, Y.; Biesold, G. M.; Cheng, Y.; Ge, M.; Li, H.; Huang, J.; Lin, Z.; Lai, Y. *Chem. Soc. Rev.* **2023**, *52* (2), 473−509.
(29) Zou, T.; Xing, X.; Yang, Y.; Wang, Z.; Wang, Z.; Zhao, R.; Zhang, X.; Wang, Y. *J. Alloys Compd.* **2020**, *825*, No. 153904.
(30) Boruah, B. D.; Misra, A. *RSC Adv.* **2015**, *5* (110), 90838−90846.

https://doi.org/10.1021/acs.analchem.5c04212
Anal. Chem. 2025, 97, 25937−25945